BMC Oral Health

RESEARCH

Open Access

Keratinocyte necroptosis promotes the progression of radiation-induced oral mucositis

Manqiong Dai[1†], Xingzhu Dai[2†], Yuee Liang[1], Xiaoyu Li[1], Huacong Huang[1] and Wanghong Zhao[1*]

Abstract

Importance Radiation-induced oral mucositis (RIOM) is a prevalent complication arising from radiation therapy for tumors or combined radiotherapy, but the therapeutic options available remain limited. Understanding its underlying mechanisms is crucial for developing effective interventions.

Objectives To investigate whether keratinocyte necroptosis contributes to RIOM pathogenesis and evaluate the effects of RIPK3/MLKL inhibition.

Methods A mouse model of RIOM was established with varying irradiation doses. Tongue tissues were analyzed via histological staining, immunohistochemistry, and Western blot. In vitro, keratinocytes were irradiated and treated with RIPK3 or MLKL inhibitors. Subsequently, cell viability, necroptosis, and inflammatory cytokine expression were assessed using CCK-8, LDH release, Western blot, flow cytometry and RT-qPCR.

Results In irradiated mouse tongues, p-RIPK3/RIPK3 and p-MLKL/MLKL ratios were significantly elevated ($P < 0.01$), accompanied by heightened expression levels of IL-1β and IL-6. Similar findings were observed in keratinocytes, which, after 12 Gy irradiation for 2.5 days, reduced cell viability ($P < 0.001$), enhanced necroptotic marker expression ($P < 0.001$), and increased inflammatory cytokine levels ($P < 0.001$). Furthermore, treatment with RIPK3 inhibitor GSK'872 or MLKL inhibitor GW806742X significantly reduced irradiation-induced keratinocyte cell death ($P < 0.001$), LDH release ($P < 0.001$) and the expression of inflammatory cytokines ($P < 0.01$).

Conclusions This study provides evidence that RIPK3/MLKL-mediated necroptosis in keratinocytes contributes to the pathogenesis of RIOM. Inhibiting this pathway reduces cell death and inflammation, suggesting a promising therapeutic target for the treatment of RIOM.

Keywords Radiation-induced oral mucositis, Keratinocytes, Inflammation, Necroptosis

[†]Manqiong Dai and Xingzhu Dai contributed equally to this work.

*Correspondence:
Wanghong Zhao
wanghong_zhao@sina.com
[1]Department of Stomatology, Nanfang Hospital, Southern Medical University, No. 1838, Guangzhou Avenue North, Guangzhou 510515, China
[2]Department of Stomatology, Guangdong Provincial People's Hospital, Guangdong Academy of Medical Sciences, Southern Medical University, Guangzhou, China

Introduction

Radiation-induced oral mucositis (RIOM), a common complication of tumor radiation therapy or combined radiotherapy, is an acute and chronic injury to the oral mucosa caused by ionizing radiation. It manifests as persistent oral mucosal erosion or ulceration, often accompanied by severe pain and diminished oral function [1]. RIOM affects over 80% of patients with head and neck cancers undergoing radiotherapy [2, 3]. The risk of developing RIOM increases with higher radiation doses [4], leading to debilitating symptoms such as oral pain, taste disturbances, and malnutrition, all of which greatly reduce patients' quality of life [3].

The pathogenesis of RIOM is complex and is typically described in five stages: initiation, upregulation and activation (primary damage response), signal amplification, ulceration, and healing [5]. Notably, keratinocyte death plays a pivotal factor in the pathogenesis of RIOM. During the progression of RIOM, ionizing radiation causes keratinocyte death, disrupting epithelial integrity and leading to ulcer formation [6]. Subsequently, in the healing phase, signals from the submucosal layer stimulate keratinocytes in the basal and part of the stratum spinosum to migrate and proliferate, promoting tissue re-epithelialization [5]. This model merely offers a fundamental framework for gaining an understanding of the condition. Consequently, further investigation into its pathogenesis is crucial to identify new treatment targets.

The mode of cell death is critical for disease progression. Current therapies for keratinocyte death in RIOM focus on apoptosis, a non-inflammatory, immunoselected and non-cleaved form of cell death [7]. However, a considerable number of inflammatory cytokines are produced during the progression of RIOM [8]. Necroptosis is a more effective mechanism for triggering inflammatory and immune responses than apoptosis. This inflammatory cell death typically results in the release of a multitude of inflammatory cytokines. To put it more specifically, necroptosis is a form of lysogenic, inflammatory cell death mediated by receptor-interacting protein kinase 3 (RIPK3), which phosphorylates mixed lineage kinase domain-like protein (MLKL) [9]. The oligomerization and translocation of phosphorylated MLKL to the plasma membrane results in cell swelling, membrane rupture, and eventual cell death [10].

As evidenced by studies, necroptosis has been found to play a crucial role in inflammatory conditions, including pancreatitis and inflammatory bowel disease [11–13]. Likewise, in the context of radiation-induced tissue damage, necroptosis has been implicated in disorders such as radiation-induced lung injury and radiation-induced intestinal injury [14, 15]. It is noteworthy that keratinocytes represent a potential cell type in which necroptosis may take place, as observed in conditions such as psoriasis [16]. Nevertheless, few studies investigating whether necroptosis occurs in keratinocytes within RIOM.

Consequently, the objective of this study was to investigate whether keratinocyte necroptosis is involved in the pathogenesis of RIOM, with the ultimate goal of providing new insights into disease mechanisms and potential therapeutic targets for its prevention and treatment.

Methods

Mice

Six- to eight-week-old male SPF C57BL/6J mice (19–23 g) were obtained from the Experimental Animal Center of Southern Medical University. The mice were housed in the Laboratory Animal Center with free access to pellet food and water. They were kept in a conventional environment with controlled temperature (22 ± 2 °C) and humidity (55 ± 10%), and a 12/12-hour day/night cycle. All experiments were conducted in accordance with the Medical Ethics Committee and Biosafety Management Committee (Ethical number: KY2024-986-02).

X-ray irradiation

The mice were divided into four groups: control (no irradiation), 9 Gy irradiation, 17 Gy irradiation, and 25 Gy irradiation ($n = 9$/group). Prior to irradiation, mice were anesthetized (Pentobarbital sodium, 50 mg/kg, IP) and measures were taken to minimize animal suffering. Mice in the control group were maintained under normal conditions throughout the study, and tongue samples were collected on days 7 and 9. The oral cavities of the mice were subjected to irradiation using the Faxitron MultiRad 225 Irradiation System. It ensured that only the oral cavity was exposed to radiation, while the remainder of the body was protected by lead shielding. Prior to irradiation, the mouse tongues were protruded gently. Mice were exposed to single-dose X-rays of 9 Gy, 17 Gy, or 25 Gy at a rate of 2 Gy/min and SSD (source-to-surface distance) of 50 cm, except for the control group. Following irradiation, the mice were allowed to recover on a heating pad before being returned to their cages. The oral mucosa was examined and weighed daily, photographs were taken every other day, and tongue samples were collected on days 7 and 9.

Evaluation of oral mucositis

Upon completion of the experiment, mice were humanely euthanized (Pentobarbital sodium, 100 mg/kg, IP), and the entire tongue was removed. Gross photographs were taken for macroscopic analysis of RIOM. The severity of tongue mucositis in mice was evaluated utilizing the VRTOG score, with the entire assessment procedure adhering to the principles of blinding and randomization. A portion of the excised tongue was stained with

0.05% toluidine blue (TB, Macklin) for 10 min and rinsed with 10% acetic acid for 5 min for further observation. After staining observations, half of the tongue tissues were stored at -80 °C for protein extraction and Western blot analysis, while the other half were fixed 4% paraformaldehyde for histological and immunohistochemical examinations.

Histological and immunohistochemistry staining

Paraffin sections were prepared for histologic analysis. The specimens were fixed in 4% paraformaldehyde, embedded in paraffin. After sections were performed, they were stained with hematoxylin and eosin (H&E) for confirm histological changes. To assess epithelial thickness, measurements were taken at different randomly selected sites from three tongue tissues. To confirm whether necroptosis occurred in the tongue tissues, immunohistochemistry was performed using monoclonal antibodies against p-MLKL (Invitrogen), IL-1β (Abclonal), and IL-6 (Abclonal). After incubation with the primary antibody described above, further incubation was performed with the appropriate horseradish peroxidase-coupled secondary antibody (Jackson ImmunoResearch; ZSGB-BIO). Subsequently, after a series of steps such as DAB (3,3'-diaminobenzidine tetrahydrochloride) staining, hematoxylin restaining, dehydration transparency, and sealing, images were captured using a slide scanner.

Cell culture and treatment

Human immortalized keratinocytes (HaCaT cells) were obtained from the American Type Culture Collection (ATCC, Manassas, VA). HaCaT cells, a commonly used model for RIOM [17, 18], were maintained in high-glucose Dulbecco's modified Eagle medium (DMEM, Gibco, Grand Island, NY) supplemented with 10% fetal bovine serum and 100 U/mL penicillin-streptomycin (Gibco, Paisley, PA) at 37 °C and 5% CO2.

HaCaT cells were treated with single-dose X-rays of 6 Gy, 12 Gy, 18 Gy, and 24 Gy at a rate of 2 Gy/min, with an SSD of 50 cm for direct irradiation. To further determine the involvement of necroptosis, irradiated cells were treated with 10 μM RIPK3-specific inhibitor GSK'872 (Selleckchem) or 2 μM MLKL-specific inhibitor GW806742X (Selleckchem), while the control cells were treated with an equal volume of dimethyl sulfoxide.

Cell viability and cytotoxicity assay

HaCaT cells were inoculated at a density of 9×10^3 cells/well in 96-well culture plates and treated with a single dose of 6 Gy, 12 Gy, 18 Gy, 24 Gy X-ray direct irradiation for 1d, 1.5d, 2d, 2.5d, 3d, 3.5d, 4d. The control wells were not subjected to any form of treatment. The viability of the cells was determined by applying the CCK-8 Cytotoxicity Assay Kit (Dojindo Laboratories). Meanwhile, the cells were pretreated with inhibitor for a period of 2 h prior to irradiation, while an equal volume of dimethyl sulfoxide was applied as a control. Cytotoxicity was evaluated using the Lactate Dehydrogenase (LDH) Assay Kit (Beyotime). The calculations of cell viability and cytotoxicity were performed in accordance with the instructions provided by the manufacturer.

Western blotting

Protein lysates were extracted from mouse tongue tissues using radioimmunoprecipitation assay (RIPA) buffer containing protease and phosphatase inhibitors (Bimake) via grinding and sonication. After quantification of proteins using the bicinchoninic acid (BCA) protein assay kit (Thermo Fisher Scientific), protein sample were electrophoresed on a 10% SDS-PAGE gel and transferred to a PVDF membrane (Bio-Rad). Following the sealing process, the membranes were blocked and incubated overnight at 4 °C with primary antibodies against RIPK3 (1:1,000, Cell Signaling Technology), p-RIPK3 (1:1,000, Cell Signaling Technology), MLKL (1:1,000, Cell Signaling Technology), p-MLKL (1:1,000, Cell Signaling Technology), and β-actin (1:5,000, Abclonal). Membranes were then incubated with horseradish peroxidase-conjugated secondary antibodies (1:3,000, Proteintech). Subsequently, immunoblots were visualized using enhanced chemiluminescence (Bio-Femto, Fudebio) and analyzed with a chemiluminescence imaging system (Tanon 5200). The optical density of the bands was ultimately quantified using the ImageJ software.

Reverse transcription-quantitative PCR

Total RNA was extracted from HaCaT cells using RNAiso Plus (TaKaRa) and quantified with a Nanodrop (Thermo Fisher Scientific). cDNA synthesis was performed using a reverse transcriptase kit (TaKaRa). The obtained templates were amplified by real-time quantitative PCR on a LightCycler 480 system (Roche) using SYBR Premix Ex Taq (TaKaRa). The relative gene expression levels of IL-1β, IL-6 and TNF-α were normalised to β-actin expression and quantified using the 2-ΔΔCT method.

Flow cytometry analysis

HaCaT cells were inoculated in 6-well cell culture plates at a density of 7×10^5 cells per well and treated with single-dose 6 Gy, 12 Gy, 18 Gy, 24 Gy X-ray direct irradiation with inhibitor. Cells were harvested after a 2.5-day irradiation period and stained with propidium iodide (PI) and fluorescein isothiocyanate (FITC)-labeled Annexin V (KeyGEN). A FACSCalibur flow cytometer (BD Biosciences) and FlowJo software were used to analyse the percentage of double positive cells.

Hoechst 33342/PI fluorescent staining

Cells were treated according to the kit instructions and double stained with Hoechst 33342 and PI (Solarbio) for 20 min at 4 °C under light protection. Fluorescent images were then captured using a fluorescence microscope (Nikon).

Statistical analysis

Each experimental condition was assessed in triplicate, and all experiments were independently repeated three times. Data were expressed as mean ± standard deviation. Statistical analysis was performed using SPSS software (version 23.0; IBM SPSS Inc.). Student's t-test was used for the comparison of two groups. A one-way analysis of variance (ANOVA) followed by a least significant difference (LSD) post hoc test was used for multiple group comparisons. Statistical significance was defined as a two-tailed P value < 0.05.

Results

Establishment of radiation-induced oral mucositis model in mice

A single - dose RIOM was initially established in irradiated mice with three doses of 9 Gy, 17 Gy, and 25 Gy. A single dose of 17 Gy or 25 Gy irradiation resulted in a considerable reduction in body weight. In the group irradiated with 17 Gy, the most noticeable weight loss occurred on day 9, followed by gradual recovery. However, the 25 Gy group experienced complete mortality by day 9 (Fig. 1A). In addition to the effects on body weight, research findings that a single dose of X-rays at 17 Gy and 25 Gy reliably caused substantial mucositis, particularly in the tongue mucosa. Mice exposed to 17 Gy showed erythema on the ventral tongue mucosa on day 3, flaky pseudomembranes on day 7, and ulceration on day 9. While Mice irradiated with 25 Gy exhibited severe oedema on day 3, followed by localized mucosal exfoliation on day 7, and ulceration on day 9 (Fig. 1B). The VRTOG score for mucositis showed a clear correlation between the severity of mucosal injury in mice not only with duration and dose, but also with body weight loss (Fig. 1C).

To assess the extent of mucositis more accurately, TB staining was employed to visualize the mucosal defects. The stained area, relative to the entire tongue area, was observed to quantify the extent of injury. TB staining revealed severe mucosal damage in the tongues of mice exposed to 17 Gy and 25 Gy, compared to controls (Fig. 1B). In contrast, mice irradiated with the 9 Gy dose exhibited minimal effects on both body weight and tongue mucosa.

Given the systemic impact on the mice and the degree of tongue mucosal damage, a single dose of 17 Gy was selected for further experiments. To further evaluate histopathological changes in the tongue mucosa, tissue sections from mice on days 7 and 9 were stained with H&E for analysis to examine the thickness of the remaining epithelium (Fig. 1D). Histological examination revealed that the integrity and continuity of the epithelial layer in the dorsal mucosa of the tongue in irradiated mice were compromised. Tongue mucosal epithelium has revealed marked atrophic changes, including thinning of the epithelial layer, loss of basal epithelial cells, and even partial epithelial ablation, particularly on day 9 post-irradiation with 17 Gy ($P < 0.001$). Similarly, the ventral lingual mucosal epithelium of these irradiated mice exhibited thinning at day 9 ($P < 0.001$) (Fig. 1E, F). Furthermore, the basal layer of the tongue mucosa in irradiated mice displayed various pathological alterations, such as cell enlargement, disordered cellular arrangement, and the infiltration of numerous inflammatory cells.

Activation of the RIPK3/MLKL signaling pathway in mice with radiation-induced oral mucositis

To explore whether necroptosis is involved in RIOM, key necroptosis markers in the tongue mucosal epithelium were further investigated. Western blot analysis revealed a significant increase in the phosphorylation of RIPK3 and MLKL on days 7 and 9 post-irradiation, and a significant increase in the p-RIPK3/RIPK3 and p-MLKL/MLKL ratios ($P < 0.01$) (Fig. 2A, B). In order to provide further clarification regarding the range of expression of key proteins associated with necroptosis, immunohistochemistry revealed strong expression of p-MLKL in both the dorsal and ventral tongue mucosa of irradiated mice, with higher expression observed on day 9 in comparison to unirradiated controls (Fig. 2C). These results indicate dysregulation of necroptosis-related pathways in the tongue mucosal epithelium of irradiated mice. Additionally, immunohistochemical staining revealed elevated levels of inflammatory cytokines IL-1β and IL-6 in the tongue mucosa of irradiated mice (Fig. 2D). Notably, p-MLKL and these inflammatory cytokines were primarily localized to keratinocytes in the upper layers of the mucosa, suggesting that radiation exposure induces overexpression of necroptotic proteins and triggers a substantial inflammatory response in keratinocytes. This finding provides evidence that inflammatory cell death is involved in the pathological mechanisms of RIOM.

Necroptosis activation in irradiated HaCaT cells

The high expression of key necroptosis-associated molecules in the lingual mucosal epithelium of mice with RIOM suggests that keratinocytes undergo necroptosis. To simulate necroptotic keratinocytes in radiation-induced oral mucositis lesions, HaCaT cells were irradiated with various radiation doses. The cell viability was assessed using CCK-8 at different time points

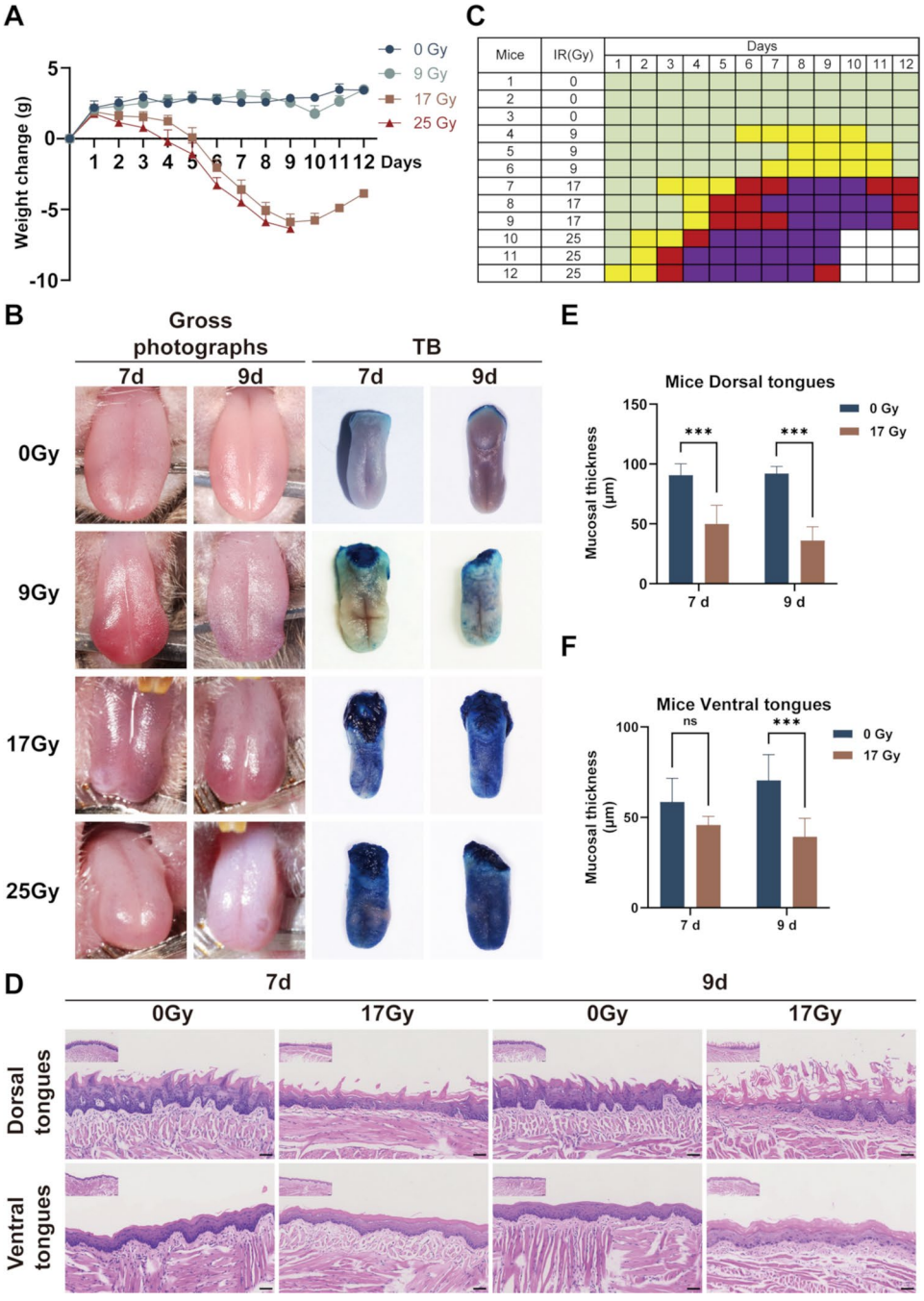

Fig. 1 Irradiation induced ulcers on the tongue mucosa of mice and establishment of a radiation-induced oral mucositis (RIOM) mouse model. (**A**) Daily body weight changes in mice following irradiation with 9, 17, and 25 Gy. (**B**) Gross photographs and TB staining of mouse tongue mucosa at days 7 and 9 post-irradiation. (**C**) VRTOG scoring of RIOM in mice. (**D**) H&E staining of the dorsal and ventral tongue mucosa in mice irradiated with 17 Gy, observed on days 7 and 9. Scale bar: low magnification 100 μm, high magnification 50 μm. (**E**, **F**) Respectively quantitative analysis of the thickness of the dorsal and ventral tongue mucosa of the above sample sections. Data are presented as mean ± SEM. Statistical significance was assessed using one-way ANOVA followed by LSD post hoc test. NS, not significantly different. *$P < 0.05$, **$P < 0.01$ and ***$P < 0.001$

in HaCaT cells. The results demonstrated a significant reduction in cell viability when cells were irradiated for more than 2.5 days ($P < 0.001$). At this time point, the cell viability of 12 Gy irradiated group had declined to 73.85%, whereas the cell viability of 24 Gy irradiated group had dropped to 69.87% (Fig. 3A). These results suggest that cell activity was suppressed in a manner dependent on both the dose of irradiation and the duration of exposure.

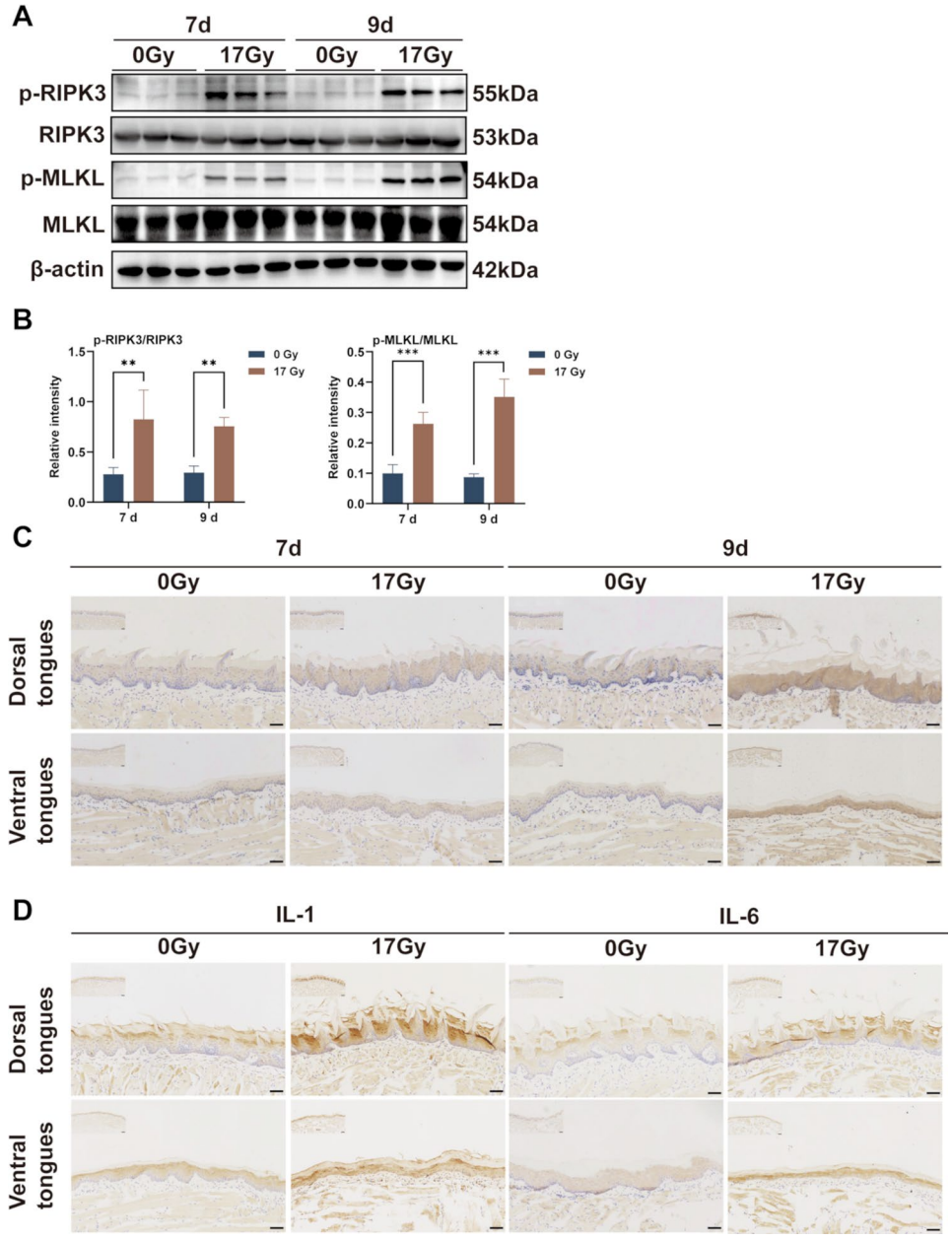

Fig. 2 Upregulation of the RIPK3/MLKL signaling pathway in mice with RIOM. (**A**) Western blot analysis of p-RIPK3, RIPK3, p-MLKL, and MLKL expression levels in tongue mucosal specimens, along with their corresponding optical density analysis (**B**). β-actin was used as an internal standard for protein normalization. Results are presented as mean ± standard deviation (SD) from three independent experiments. Statistical significance was assessed using one-way ANOVA followed by LSD post hoc test. $^{*}P < 0.05$, $^{**}P < 0.01$ and $^{***}P < 0.001$. (**C**) Representative immunohistochemical staining of p-MLKL in tongue tissue of irradiated mice. Scale bar: low magnification 100 μm, high magnification50 μm. (**D**) Representative immunohistochemical staining of the inflammatory cytokines IL-1, IL-6 in tongue tissue of irradiated mice. Scale bar: low magnification 100 μm, high magnification 50 μm

Furthermore, at 2.5 days post-irradiation, the expression levels of inflammatory markers IL-1β, IL-6, and TNF-α in HaCaT cells were progressively elevated with increasing radiation doses, with the higher expression observed at 12 Gy ($P < 0.001$) (Fig. 3B). The expression of these inflammatory markers in HaCaT cells was also measured at different time points in cells irradiated with 12 Gy, showing a time-dependent increase, peaking at 2.5 days post-irradiation ($P < 0.001$) (Fig. 3C). These findings indicate that irradiation induces inflammatory cell death in HaCaT cells in a dose- and time-dependent manner.

To determine whether radiation triggers necroptosis via the RIPK3/MLKL signaling pathway, samples were collected 2.5 days after irradiation at different doses. Western blot analysis revealed that phosphorylation of the necroptosis-related proteins RIPK3 and MLKL began

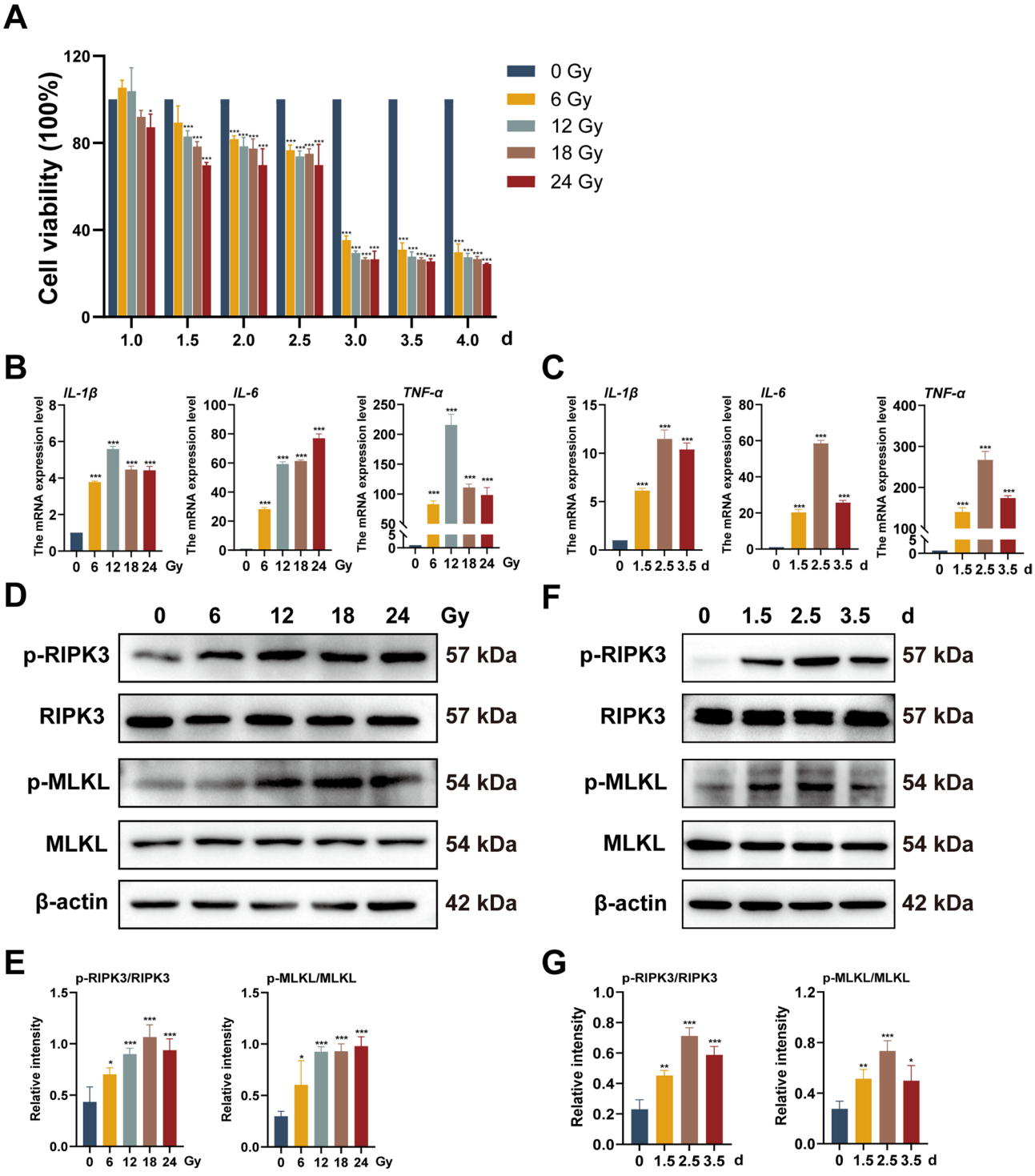

Fig. 3 Radiation-induced necroptosis in HaCaT cells. (**A**) Effect of irradiation on HaCaT cell viability. (**B** and **C**) Expression of mRNA for inflammatory cytokines, including IL-1β, IL-6 and TNF-α, following (**B**) different irradiation doses (Gy) and (**C**) different time points. (**D**) Western blot analysis of p-RIPK3, RIPK3, p-MLKL, and MLKL expression in HaCaT cells 2.5 days post-irradiation at different doses and (**E**) respective optical density analysis. (**F**) Western blot analysis of necroptotic markers in HaCaT cells irradiated with 12 Gy at various time points and (**G**) respective optical density analysis. β-actin was used as an internal standard for protein normalization. Results are shown as ± SD means of three replicates from three independent experiments. Statistical significance was determined using one-way ANOVA and LSD post hoc tests. *$P < 0.05$, **$P < 0.01$ and ***$P < 0.001$

to increase in HaCaT cells irradiated with a single 6 Gy dose, with higher expression observed in cells irradiated with 12 Gy (Figs. 3D, E). The ratios of p-RIPK3/RIPK3 and p-MLKL/MLKL exhibited a notable increase at the 12 Gy dose ($P < 0.001$). Additionally, elevated phosphorylation of RIPK3 and MLKL was detected at 1.5 days after 12 Gy irradiation, reaching peak levels at 2.5 days ($P < 0.001$) (Figs. 3F, G). Based on these results, a single 12 Gy irradiation followed by 2.5 days of incubation was chosen for subsequent experiment. Taken together, these data suggest that radiation induces necroptosis in keratinocytes through activation of the RIPK3/MLKL signaling pathway.

Inhibition of RIPK3/MLKL attenuates radiation-induced necroptosis in vitro

To further determine the effect of necroptosis in radiation-induced cell death and inflammation, HaCaT cells were treated with either the RIPK3 inhibitor GSK'872 or the MLKL inhibitor GW806742X before irradiation. The release of LDH from HaCaT cells subjected to irradiation increased, reaching a level of 37.11%. However, upon treatment with the GSK'872 inhibitor, this LDH release was significantly curtailed, dropping to 16.80% ($P < 0.001$). Similarly, in irradiated cells treated with the GW806742X inhibitor, LDH release was also mitigated, decreasing to 14.47% ($P < 0.001$). These findings collectively indicate that the inhibition of RIPK3 and MLKL is effective in preventing LDH release (Fig. 4A). Furthermore, the proportion of cells exhibiting double-positivity for annexin V and propidium iodide, as induced by irradiation, increased to 22.30%. In contrast, this proportion decreased significantly following inhibitor treatment ($P < 0.001$) (Fig. 4B, C).

Similarly, Hoechst 33342/PI double staining further confirmed that GSK'872 or GW806742X substantially reduced the proportion of necrotic cells in the irradiated group (Fig. 4D). These results suggest that the inhibition of RIPK3 or MLKL can effectively mitigate radiation-induced necroptosis. To further explore the anti-inflammatory effects of the two inhibitors in HaCaT cells, qRT-PCR was performed to analyse the mRNA expression of inflammatory cytokines, including IL-1β, IL-6 and TNF-α, which were significantly reduced upon inhibitor treatment ($P < 0.01$) (Fig. 4E, F). Overall, these findings demonstrate that inhibiting RIPK3 or MLKL not only prevents necroptosis but also attenuates the inflammatory response induced by radiation in HaCaT cells.

Discussion

Dysregulated inflammatory responses and keratinocyte death are crucial in the pathophysiology of RIOM [19]. The current study shows that necroptosis occurs in RIOM, with the necroptosis-related protein p-MLKL predominantly expressed and localized in the tongue mucosal epithelium, especially in keratinocytes. Inhibition of necroptosis markedly reduced cell death and inflammatory responses in this context.

Necroptosis has been identified as a key factor in the pathogenesis of various diseases, including infections [20], inflammatory conditions [21], neurodegenerative disorders [22], and cancer [23]. When necroptosis is uncontrolled, it leads to the release of damage-associated molecular pattern (DAMP) molecules, which trigger systemic immune responses and contribute to tissue damage [24, 25]. Recently, there has been growing attention to the role of necroptosis in oral diseases, as evidenced by research on periodontitis [26, 27]. Preliminary work by our team has also observed necroptosis in refractory apical periodontitis [20]. In the case of RIOM, this study found that irradiated keratinocytes exhibited increased cell death and higher levels of inflammatory cytokines. Furthermore, inhibition of RIPK3 or MLKL reduced both cell death and inflammatory cytokines secretion.

The phosphorylation status of RIPK3 and MLKL is a commonly employed method for the assessment of necroptosis [28]. In this study, elevated expression of the necroptosis markers p-RIPK3 and p-MLKL was detected in the tongues of mice with RIOM, suggesting that keratinocytes undergo necroptosis during the progression of RIOM. While MLKL is an executioner protein of necroptosis [29], phosphorylation of MLKL alone may not fully indicate necroptosis activation [30]. This study confirmed that inhibiting necroptosis-related proteins, using the RIPK3 inhibitor GSK'872 and the MLKL inhibitor GW806742X, significantly reduced cell death and inflammation in vitro, highlighting the occurrence of necroptosis in radiation-induced keratinocytes.

RIPK3 (receptor-interacting protein kinase 3) is a pivotal component of the necrosome [31, 32], which classically functions to stimulate MLKL activation and trigger necroptosis [33, 34]. Furthermore, RIPK3 kinase activity has the potential to activate the NLRP3 inflammasome through RIPK3/MLKL signal, leading to IL-1β secretion [35, 36]. It is noteworthy that RIPK3 has the capacity to induce inflammation and cell death through a non-classical pathway that is independent of necroptosis. RIPK3 has been demonstrated to mediate inflammation by inducing cytokines and chemokines in cells to promote neutrophil recruitment in a manner that is not dependent on necroptosis [37]. Additionally, RIPK3 has been demonstrated to facilitate the NLRP3-caspase1 signaling axis triggering GSDMD activity and IL-1β-driven inflammation, whereas these responses are independent of its substrate MLKL and necroptosis [35]. Flow cytometry analysis revealed that treatment with GSK'872 resulted in a lower proportion of double-positive cells for Annexin V and PI, in comparison to GW806742X treatment. This

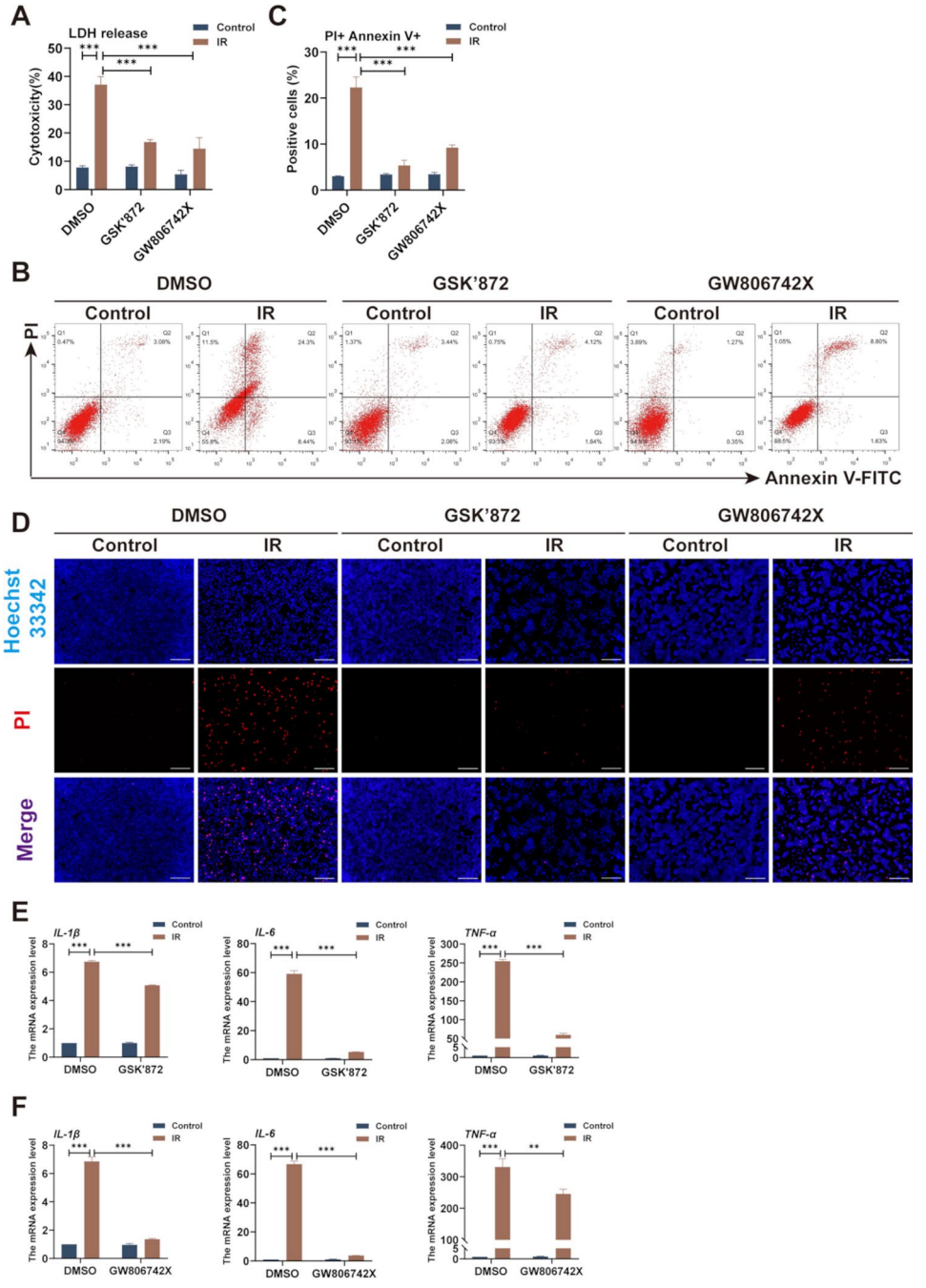

Fig. 4 Pretreatment with RIPK3 inhibitor or MLKL inhibitor reduces radiation-induced cell death and inflammation. (**A**) Lactate dehydrogenase (LDH) release was measured in HaCaT cells cultured for 2.5 days post-irradiation with a dose of 12 Gy, in the presence or absence of the RIPK3 inhibitor GSK'872 or the MLKL inhibitor GW806742X. (**B**) Flow cytometry analysis of HaCaT cells stained with propidium iodide (PI) and annexin V, and (**C**) quantification of double-positive cells (PI and annexin V staining). (**D**) Representative fluorescent images of Hoechst 33342 (blue) and PI (red) double staining. Scale bar: 100 μm. (**E**, **F**) The mRNA expression levels of inflammatory cytokines by qRT-PCR, including IL-1β, IL-6, and TNF-α. Results are shown as ± SD means of three replicates from three independent experiments. Statistical significance was determined using one-way ANOVA and LSD post hoc tests. *$P < 0.05$, **$P < 0.01$ and ***$P < 0.001$

was further supported by Hoechst 33342/PI double fluorescence staining. These findings suggest that GSK'872 may inhibit non-classical RIPK3 pathways that are independent of necroptosis.

Prior research has demonstrated that MLKL functions as an execution protein for necroptosis, which can be triggered by oligomerization, phosphorylation and membrane binding of MLKL [38]. Additionally, MLKL can undergo translocation in such a way that it triggers

membrane damage, potassium efflux and NLRP3 activation to drive IL-1β secretion, a phenomenon that is not death-induced DAMP release results [39]. Therefore, the translocation of MLKL to the plasma membrane is important, yet it does not fully elucidate its multifaceted role within the cell. Further studies have demonstrated that activated MLKL is capable of translocating to multiple intracellular compartments, in addition to translocating to and disrupting the plasma membrane. These include mitochondria [40], lysosomes [41], the Golgi apparatus [42] and endosomes [43]. Furthermore, it has been demonstrated that MLKL facilitates its own release from extracellular vesicles by interacting with endosomal sorting complexes required for transport (ESCRT) proteins [44]. Consequently, these findings emphasize that MLKL modulates its own cellular localization, thereby influencing cellular function or mediating cell-cell interactions, which in turn regulate disease progression. Interestingly, the present study revealed that the MLKL inhibitor GW806742X exhibited a more pronounced inhibitory effect on irradiation-induced IL-1β inflammatory responses when compared with the RIPK3 inhibitor GSK'872. Therefore, it can be postulated that upon activation, MLKL may initiate a mechanism that facilitates IL-1β release by translocating to other intracellular compartments, an event that is independent of necroptosis. In conclusion, further studies are required to gain a more comprehensive understanding of the role of MLKL in the regulation of cell death, with a view to uncovering other mechanisms involved in its activation and function. Nevertheless, this study identifies a pivotal function for RIPK3/MLKL in radiation-induced inflammation and tissue damage, indicating that RIPK3 and MLKL may be promising targets for further investigation.

Notably, different cell death pathways can be viewed as a single cell death process, but multiple cell death modalities may occur in the same disease. Similarly, this study verified that keratinocytes underwent apoptosis by Annexin V-FITC/PI flow cytometry analysis, consistent with previous studies [7], which suggests the presence of a mixed type of death consisting of apoptosis and necroptosis. Additionally, the study revealed that NLRP3 inflammatory vesicles play a pivotal role in radiation-induced mucosal injury [45]. This indicates that apoptosis, pyroptosis, and necroptosis are all involved in the pathological process of RIOM. An increasing body of evidence now emphasizes that there is extensive crosstalk between cell death modalities under specific conditions, with the potential for them to regulate each other [46, 47]. Therefore, exploring how apoptosis, pyroptosis, and necroptosis interact and influence disease progression in RIOM is an attractive direction for future research.

The above findings indicate that keratinocyte necroptosis plays a pivotal role in the inflammatory cascade of RIOM, but limitations remain. Firstly, although this study demonstrated the involvement of necroptosis in the pathogenesis of RIOM, the upstream regulatory mechanisms leading to keratinocyte necroptosis remain incompletely elucidated. Future investigations using transcriptomic or proteomic profiling may help identify upstream regulators or signaling pathways, thereby facilitating the development of targeted therapies. Secondly, the in vitro experiments within this study concentrated on the cellular level, which do not fully recapitulate the structural and functional complexity of the oral mucosa. Advanced 3D culture systems such as organoid models may offer more physiologically relevant platforms for studying RIOM. Thirdly, mouse model do not fully replicate the human condition, particularly in terms of immune response. Therefore, further validation in humanized models would enhance the translational relevance of findings. Nonetheless, this study indicate that the inhibition of necroptosis with GSK'872 and GW806742X attenuates radiation-induced keratinocyte death and inflammation, highlighting the potential of necroptosis as a therapeutic target in RIOM.

Conclusions

Overall, this study clarifies that necroptosis occurs in keratinocytes in RIOM, enriches mechanistic studies of oral mucositis, and highlights the potential of inhibiting keratinocyte necroptosis as a therapeutic target for RIOM.

Author contributions

Manqiong Dai: Conceptualization, Methodology, Data curation, Formal analysis, Visualization, Writing– original draft, Writing– review & editing; Xingzhu Dai: Conceptualization, Methodology, Data curation, Formal analysis, Funding acquisition, Visualization, Writing– original draft, Writing– review & editing; Yuee Liang: Data curation, Writing– review & editing; Xiaoyu Li: Data curation, Writing– review & editing; Huacong Huang: Data curation, Writing– review & editing; Wanghong Zhao: Conceptualization, Funding acquisition, Project administration, Supervision, Writing– review & editing.

Funding

This work was supported by grants from the National Natural Science Foundation of China (82270965), the Natural Science Foundation of Guangdong Province (2024A1515013037), the Guangdong Medical Science and Technology Research Foundation (A2024079), and the Science and Technology Projects in Guangzhou (2025A04J4750).

Data availability

The datasets supporting the conclusions of this article are included within the manuscript and the supplementary materials.

Declarations

Ethical statement

The procedures for care and use of animals were approved by the Medical Ethics Committee and Biosafety Management Committee (Ethical number: KY2024-986-02) and all applicable institutional and governmental regulations concerning the ethical use of animals were followed.

Consent for publication

Not applicable.

Competing interests
The authors declare no competing interests.

Clinical trial number
Not applicable.

Received: 5 January 2025 / Accepted: 26 May 2025
Published online: 07 June 2025

References

1. Trotti A, Bellm LA, Epstein JB, Frame D, Fuchs HJ, Gwede CK, Komaroff E, Nalysnyk L, Zilberberg MD. Mucositis incidence, severity and associated outcomes in patients with head and neck cancer receiving radiotherapy with or without chemotherapy: a systematic literature review. Radiotherapy Oncology: J Eur Soc Therapeutic Radiol Oncol. 2003;66(3):253–62.
2. Mortensen HR, Overgaard J, Specht L, Overgaard M, Johansen J, Evensen JF, Andersen LJ, Andersen E, Grau C. Prevalence and peak incidence of acute and late normal tissue morbidity in the DAHANCA 6&7 randomised trial with accelerated radiotherapy for head and neck cancer. Radiotherapy Oncology: J Eur Soc Therapeutic Radiol Oncol. 2012;103(1):69–75.
3. Chow LQM. Head and neck cancer. N Engl J Med. 2020;382(1):60–72.
4. Li K, Yang L, Xin P, Chen Y, Hu QY, Chen XZ, Chen M. Impact of dose volume parameters and clinical factors on acute radiation oral mucositis for locally advanced nasopharyngeal carcinoma patients treated with concurrent intensity-modulated radiation therapy and chemoradiotherapy. Oral Oncol. 2017;72:32–7.
5. Elad S, Yarom N, Zadik Y, Kuten-Shorrer M, Sonis ST. The broadening scope of oral mucositis and oral ulcerative mucosal toxicities of anticancer therapies. Cancer J Clin. 2022;72(1):57–77.
6. Gruber S, Dörr W. Tissue reactions to ionizing radiation-oral mucosa. Mutat Res Reviews Mutat Res. 2016;770(Pt B):292–8.
7. Liang L, Gan M, Miao H, Liu J, Liang C, Qin J, Ruan K, Zhu H, Zhong J, Lin Z. Thalidomide attenuates radiation-induced apoptosis and pro-inflammatory cytokine secretion in oral epithelial cells by promoting LZTS3 expression. J Translational Med. 2024;22(1):863.
8. Maxwell CA, Fleisch MC, Costes SV, Erickson AC, Boissière A, Gupta R, Ravani SA, Parvin B, Barcellos-Hoff MH. Targeted and nontargeted effects of ionizing radiation that impact genomic instability. Cancer Res. 2008;68(20):8304–11.
9. Holen S. The radicular groove. J Am Dent Assoc (1939). 1978;97(3):441.
10. Galluzzi L, Kepp O, Chan FK, Kroemer G. Necroptosis: mechanisms and relevance to disease. Annu Rev Pathol. 2017;12:103–30.
11. Chen AQ, Fang Z, Chen XL, Yang S, Zhou YF, Mao L, Xia YP, Jin HJ, Li YN, You MF, et al. Microglia-derived TNF-α mediates endothelial necroptosis aggravating blood brain-barrier disruption after ischemic stroke. Cell Death Dis. 2019;10(7):487.
12. Caccamo A, Branca C, Piras IS, Ferreira E, Huentelman MJ, Liang WS, Readhead B, Dudley JT, Spangenberg EE, Green KN, et al. Necroptosis activation in Alzheimer's disease. Nat Neurosci. 2017;20(9):1236–46.
13. Kondylis V, Pasparakis M. RIP kinases in liver cell death, inflammation and cancer. Trends Mol Med. 2019;25(1):47–63.
14. Ding Y, Ma L, He L, Xu Q, Zhang Z, Zhang Z, Zhang X, Fan R, Ma W, Sun Y, et al. A strategy for attenuation of acute radiation-induced lung injury using crocetin from gardenia fruit. Biomed pharmacotherapy = Biomedecine Pharmacotherapie. 2022;149:112899.
15. Xu Y, Tu W, Sun D, Chen X, Ge Y, Yao S, Li B, Zhenbo Z, Liu Y. Nrf2 alleviates radiation-induced rectal injury by inhibiting of necroptosis. Biochem Biophys Res Commun. 2021;554:49–55.
16. Duan X, Liu X, Liu N, Huang Y, Jin Z, Zhang S, Ming Z, Chen H. Inhibition of keratinocyte necroptosis mediated by RIPK1/RIPK3/MLKL provides a protective effect against psoriatic inflammation. Cell Death Dis. 2020;11(2):134.
17. Kim HJ, Kang SU, Lee YS, Jang JY, Kang H, Kim CH. Protective effects of N-acetylcysteine against radiation-induced oral mucositis in vitro and in vivo. Cancer Res Treat. 2020;52(4):1019–30.
18. Jiang SJ, Xiao X, Li J, Mu Y. Lycium barbarum polysaccharide-glycoprotein ameliorates ionizing radiation-induced epithelial injury by regulating oxidative stress and ferroptosis via the Nrf2 pathway. Free Radic Biol Med. 2023;204:84–94.
19. Sonis ST. The pathobiology of mucositis. Nat Rev Cancer. 2004;4(4):277–84.
20. Dai X, Ma R, Jiang W, Deng Z, Chen L, Liang Y, Shao L, Zhao W. Enterococcus faecalis-induced macrophage necroptosis promotes refractory apical periodontitis. Microbiol Spectr. 2022;10(4):e0104522.
21. Pasparakis M, Vandenabeele P. Necroptosis and its role in inflammation. Nature. 2015;517(7534):311–20.
22. Yuan J, Amin P, Ofengeim D. Necroptosis and RIPK1-mediated neuroinflammation in CNS diseases. Nat Rev Neurosci. 2019;20(1):19–33.
23. Gong Y, Fan Z, Luo G, Yang C, Huang Q, Fan K, Cheng H, Jin K, Ni Q, Yu X, et al. The role of necroptosis in cancer biology and therapy. Mol Cancer. 2019;18(1):100.
24. Zindel J, Kubes P. DAMPs, PAMPs, and lamps in immunity and sterile inflammation. Annu Rev Pathol. 2020;15:493–518.
25. Marchi S, Guilbaud E, Tait SWG, Yamazaki T, Galluzzi L. Mitochondrial control of inflammation. Nat Rev Immunol. 2023;23(3):159–73.
26. Zhang K, Chen X, Zhou R, Chen Z, Wu B, Qiu W, Fang F. Inhibition of gingival fibroblast necroptosis mediated by RIPK3/MLKL attenuates periodontitis. J Clin Periodontol. 2023;50(9):1264–79.
27. Yang Y, Wang L, Zhang H, Luo L. Mixed lineage kinase domain-like pseudokinase-mediated necroptosis aggravates periodontitis progression. J Mol Med. 2022;100(1):77–86.
28. Weinlich R, Oberst A, Beere HM, Green DR. Necroptosis in development, inflammation and disease. Nat Rev Mol Cell Biol. 2017;18(2):127–36.
29. Zhu X, Yang N, Yang Y, Yuan F, Yu D, Zhang Y, Shu Z, Nan N, Hu H, Liu X, et al. Spontaneous necroptosis and autoinflammation are blocked by an inhibitory phosphorylation on MLKL during neonatal development. Cell Res. 2022;32(4):407–10.
30. Mishra PK, Adameova A, Hill JA, Baines CP, Kang PM, Downey JM, Narula J, Takahashi M, Abbate A, Piristine HC, et al. Guidelines for evaluating myocardial cell death. Am J Physiol Heart Circ Physiol. 2019;317(5):H891–922.
31. Daniels BP, Kofman SB, Smith JR, Norris GT, Snyder AG, Kolb JP, Gao X, Locasale JW, Martinez J, Gale M, Jr., et al. The Nucleotide sensor ZBP1 and kinase RIPK3 induce the enzyme IRG1 to promote an antiviral metabolic state in neurons. Immunity. 2019;50(1):64–76.e64.
32. Rickard JA, O'Donnell JA, Evans JM, Lalaoui N, Poh AR, Rogers T, Vince JE, Lawlor KE, Ninnis RL, Anderton H, et al. RIPK1 regulates RIPK3-MLKL-driven systemic inflammation and emergency hematopoiesis. Cell. 2014;157(5):1175–88.
33. Moriwaki K, Chan FK. RIP3: a molecular switch for necrosis and inflammation. Genes Dev. 2013;27(15):1640–9.
34. He S, Wang L, Miao L, Wang T, Du F, Zhao L, Wang X. Receptor interacting protein kinase-3 determines cellular necrotic response to TNF-alpha. Cell. 2009;137(6):1100–11.
35. Lawlor KE, Khan N, Mildenhall A, Gerlic M, Croker BA, D'Cruz AA, Hall C, Kaur Spall S, Anderton H, Masters SL, et al. RIPK3 promotes cell death and NLRP3 inflammasome activation in the absence of MLKL. Nat Commun. 2015;6:6282.
36. Kang TB, Yang SH, Toth B, Kovalenko A, Wallach D. Caspase-8 blocks kinase RIPK3-mediated activation of the NLRP3 inflammasome. Immunity. 2013;38(1):27–40.
37. Honda T, Yamamoto O, Sawada Y, Egawa G, Kitoh A, Otsuka A, Dainichi T, Nakajima S, Miyachi Y, Kabashima K. Receptor-interacting protein kinase 3 controls keratinocyte activation in a necroptosis-independent manner and promotes psoriatic dermatitis in mice. J Allergy Clin Immunol. 2017;140(2):619–22.e616.
38. Zhang DW, Shao J, Lin J, Zhang N, Lu BJ, Lin SC, Dong MQ, Han J. RIP3, an energy metabolism regulator that switches TNF-induced cell death from apoptosis to necrosis. Sci (New York NY). 2009;325(5938):332–6.
39. Conos SA, Chen KW, De Nardo D, Hara H, Whitehead L, Núñez G, Masters SL, Murphy JM, Schroder K, Vaux DL, et al. Active MLKL triggers the NLRP3 inflammasome in a cell-intrinsic manner. Proc Natl Acad Sci USA. 2017;114(6):E961–9.
40. Deragon MA, McCaig WD, Truong PV, Metz KR, Carron KA, Hughes KJ, Knapp AR, Dougherty MJ, LaRocca TJ. Mitochondrial trafficking of MLKL, Bak/Bax, and Drp1 is mediated by RIP1 and ROS which leads to decreased mitochondrial membrane integrity during the hyperglycemic shift to necroptosis. Int J Mol Sci. 2023;24(10).
41. Liu S, Li Y, Choi HMC, Sarkar C, Koh EY, Wu J, Lipinski MM. Lysosomal damage after spinal cord injury causes accumulation of RIPK1 and RIPK3 proteins and potentiation of necroptosis. Cell Death Dis. 2018;9(5):476.
42. Wu X, Fan X, McMullen MR, Miyata T, Kim A, Pathak V, Wu J, Day LZ, Hardesty JE, Welch N, et al. Macrophage-derived MLKL in alcohol-associated liver disease: regulation of phagocytosis. Hepatology (Baltimore MD). 2023;77(3):902–19.

43. Yoon S, Bogdanov K, Wallach D. Site-specific ubiquitination of MLKL targets it to endosomes and targets Listeria and Yersinia to the lysosomes. Cell Death Differ. 2022;29(2):306–22.
44. Yoon S, Kovalenko A, Bogdanov K, Wallach D. MLKL, the protein that mediates necroptosis, also regulates endosomal trafficking and extracellular vesicle generation. Immunity. 2017;47(1):51–65.e57.
45. Liu YG, Chen JK, Zhang ZT, Ma XJ, Chen YC, Du XM, Liu H, Zong Y, Lu GC. NLRP3 inflammasome activation mediates radiation-induced pyroptosis in bone marrow-derived macrophages. Cell Death Dis. 2017;8(2):e2579.
46. Samir P, Malireddi RKS, Kanneganti TD. The PANoptosome: a deadly protein complex driving pyroptosis, apoptosis, and necroptosis (PANoptosis). Front Cell Infect Microbiol. 2020;10:238.
47. Zheng M, Kanneganti TD. The regulation of the ZBP1-NLRP3 inflammasome and its implications in pyroptosis, apoptosis, and necroptosis (PANoptosis). Immunol Rev. 2020;297(1):26–38.

Publisher's note